DANMARKS OG GRØNLANDS GEOLOGISKE UNDERSØGELSE RAPPORT 2005/17

Rock physics analysis of sonic velocities in wells Lopra-1, Glyvursnes-1 and Vestmanna-1

Contribution to the SeiFaBa project Funded by the Sindri Group

Gary Mavko & Peter Japsen

GEOLOGICAL SURVEY OF DENMARK AND GREENLAND
MINISTRY OF THE ENVIRONMENT

G E U S

DANMARKS OG GRØNLANDS GEOLOGISKE UNDERSØGELSE RAPPORT 2005/17

Rock physics analysis of sonic velocities in wells Lopra-1, Glyvursnes-1 and Vestmanna-1

Contribution to the SeiFaBa project
Funded by the Sindri Group

Gary Mavko[1] & Peter Japsen[2]

[1]Stanford University, [2] GEUS

Released 01.01.2008

GEOLOGICAL SURVEY OF DENMARK AND GREENLAND
MINISTRY OF THE ENVIRONMENT

GEUS

Contents

Introduction

In this report we compare and discuss well-log observations from wells Lopra-1, Glyvursnes-1, and Vestmanna-1. Our emphasis is on sonic properties, and how they relate to depth, composition, and pore space properties. We find some differences among the wells in diagnostic rock physics crossplots, which indicate possible differences in porosity, pore texture, and mineralogy.

Data and stratigraphic interpretation

A detailed stratigraphy of basalt flows, sediment/tuff layers and dolerite dykes was established for the Lopra-1 hole drilled in 1981 based on drill cuttings and cores and compared with the density, porosity, resistivity and gamma ray log-response (Hald & Waagstein 1984; Nielsen *et al*. 1984). A more extensive logging program including a full wave sonic log was run in the deepened hole from 200 m to TD. The new logs have been used to establish a detailed stratigraphy for the flood basalt sequence between 200 m and 2500 m by dividing the lava flows into massive and porous parts (Boldreel 2003). 52 intervals with >1% potassium were mapped at the flow boundaries and interpreted as altered basalt or tuffaceous sediments. These intervals were also identified from the high values of neutron porosity and caliper in combination with low values of density, P- and S-velocity. Preliminary rock physics analysis of the Lopra-1 data were presented by Mavko et al. (2004) and by Japsen et al. (*in press*).

The stratigraphy of the basalts in the Glyvursnes-1 and Vestmanna-1 wells was established from the full core in these wells (Waagstein 1983; Waagstein & Andersen 2003). Note that the processing of the full wave sonic log for these two wells was difficult and several attempts were made before the final solution was chosen (see Waagstein & Andersen 2003).

Introduction- basic observations

Figures 1-3 show well logs from the three wells. Three facies are highlighted in color: topflows (red), massives (blue), and sediments (green). In Lopra-1 (Figure 1) we observe that the gamma ray log is systematically higher in the sediments than in the various basalt layers. The bulk density shows large fluctuations with depth, indicating primarily large variations in porosity. However, the upper limit of density is fairly uniform with depth and probably indicates that the density asymptotically approaches the mineral density as the porosity approaches zero. A line showing the expected density for pyroxene mineral is shown for reference. The lowest density values likely correspond to high porosity and/or caliper anomalies (bad hole). The sonic Vp is highest for the massive basalts, intermediate for the basalt topflows, and lowest for the sediments.

In Glyvursnes-1 (Figure 2) the gamma ray again is systematically higher for the sediments. The P-wave sonic is highest in the massives and lowest in the sediments. The bulk density is systematically lower than in Lopra-1, indicating systematically higher porosity, and possibly a different mineralogy. The density also shows smaller fluctuations than were observed in Lopra-1. Horizontal lines at 45 m and 300 m indicate distinct changes in the character of the logs (the interface between the Upper and the Middle Basalt Formations is at 355 m; Waagstein & Andersen 2003).

In Vestmanna-1 (Figure 3) the gamma ray is systematically higher in the sediments than the basalts, as with the other wells. The density and density fluctuations are smaller than in Lopra-1, similar to Glyvursnes-1. The density is lower in Vestmanna-1 (Middle Basalt Formation) than in Lopra-1 (Lower Basalt Formation). This density difference may reflect the differences in mineralogy of the two formations that has been shown from other data (Hald & Waagstein 1984; Nielsen et al. 1988). Again, the P-wave sonic is highest in the massives and lowest in the sediments. The Vp/Vs ratio in Vestmanna-1 is much more uniform than in either Lopra-1 or Glyvursnes-1, though there are abrupt Vp/Vs spikes.

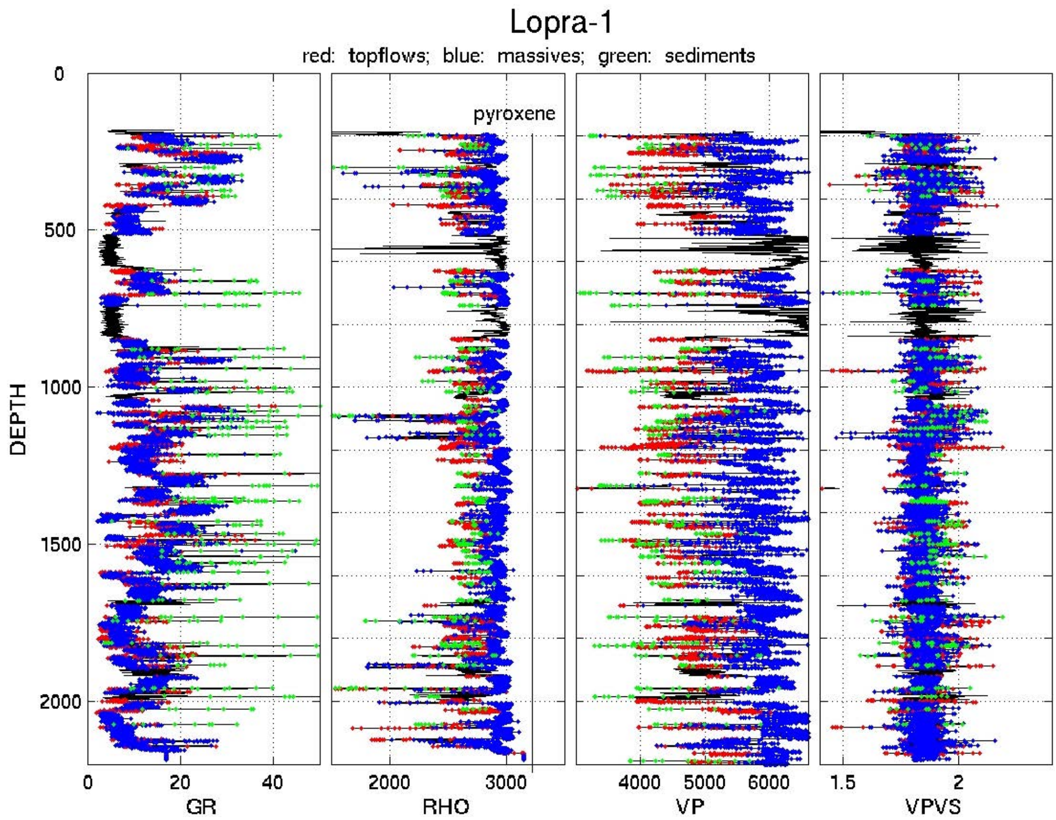

Figure 1. *Log curves for Lopra-1. Topflows are highlighted in red; massives, blue; and sediments, green.*

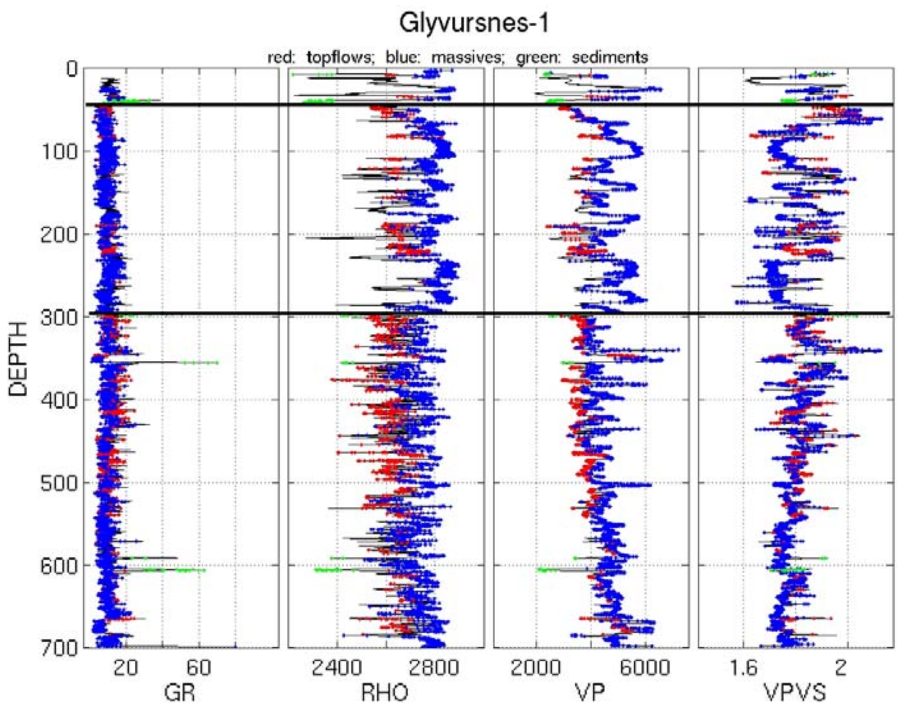

Figure 2. *Log curves for Glyvursnes-1. Topflows are highlighted in red; massives, blue; and sediments, green. Black lines mark changes in log pattern.*

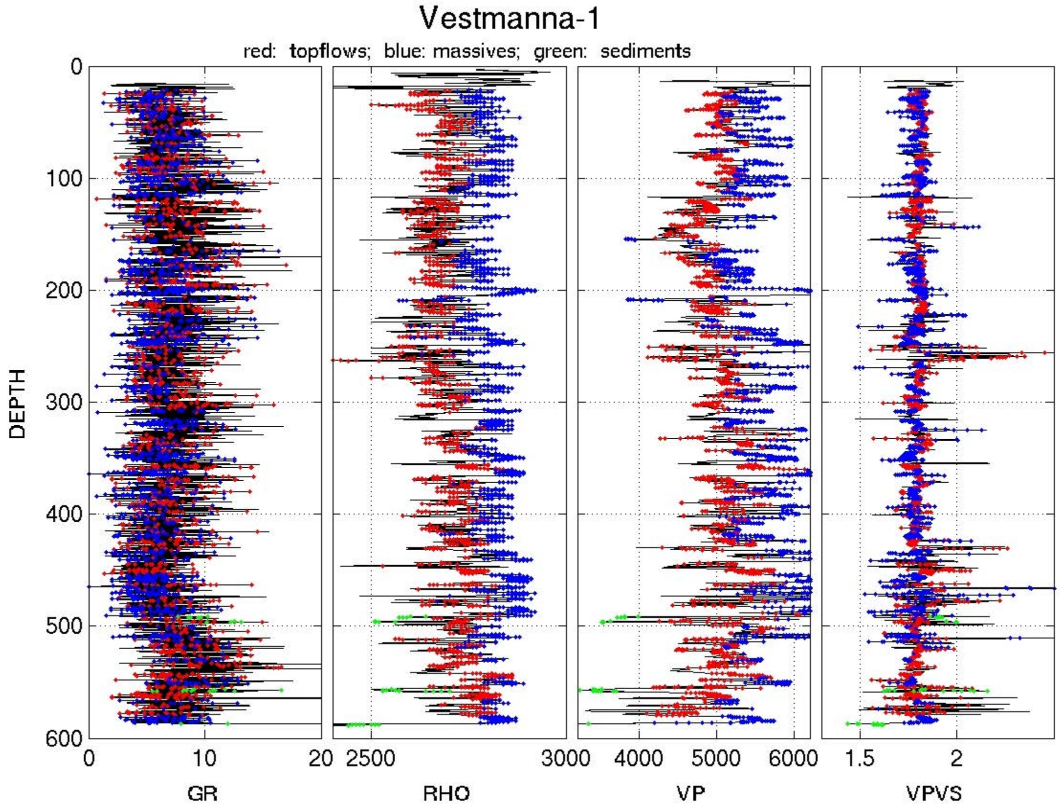

Figure 3. *Log curves for Vestmanna-1. Topflows are highlighted in red; massives, blue; and sediments, green.*

Figures 4-6 show sonic Vp vs. Vs in wells Lopra-1, Glyvursnes-1, and Vestmanna-1. The empirical Greenberg-Castagna (1992) lines for water-saturated sandstone, shale, dolomite, and limestone are shown for comparison. Although none of the curves was developed for basalt, they provide a reference. These plots illustrate that sonic data are often extremely well correlated in the Vp vs. Vs plane, with slopes that reflect the rock composition and pore fluids. In each plot we also show linear regressions (dashed black lines) to the basalt data shown. It is interesting that for each well, the slopes of the basalt regressions are different.

For each of the Greenberg-Castagna lithologic curves, as well as for the basalt regression, the upper right extent can be interpreted as approximately the mineral point, at zero porosity. (Strictly speaking, none of these curves pass exactly through the mineral point. The reason is that the curves are empirical fits to data, and none of those data came close to zero porosity.) Moving to the lower left along each curve corresponds to increasing total porosity. The left-most intercept, at Vs=0 can be thought of as critical porosity, where the rock is falling apart. (Again, the precise Vp intercept value of the lines is not exactly what we would expect for a mineral-water suspension at critical porosity; the explanation again is that this high porosity limit is an extrapolation of the empirical curves beyond their range of validity.)

We observe in Figures 4-6 that the data from Lopra-1 and Vestmanna-1 have similar regressions, with Vp/Vs larger than in Glyvursnes-1. The data in Glyvursnes-1 span the larg-

est range of velocities, while those in Vestmanna-1 span the narrowest range. The average velocities in Lopra-1 and Vestmanna-1 are slightly higher than in Glyvursnes-1.
Another observation is that all three facies fall roughly along the same trends in Figures 4-6. This implies (but does not guarantee) that the rocks have similar compositions (or at least similar mineral elastic properties).

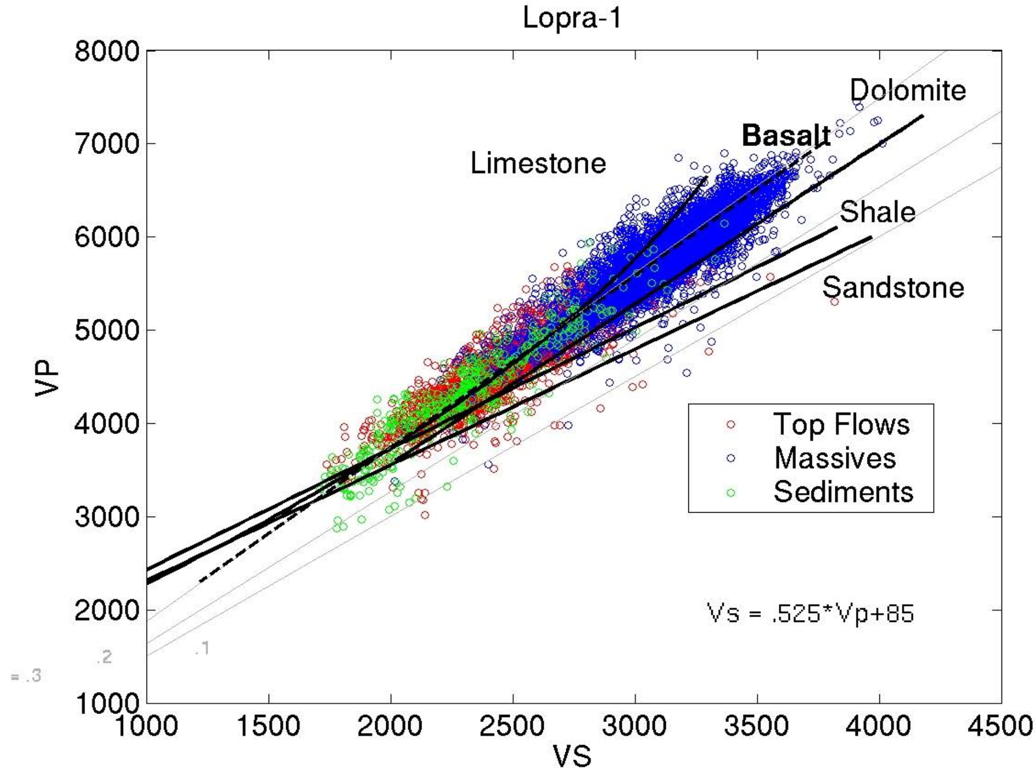

Figure 4. *Sonic Vp vs. Vs for Lopra-1. Empirical curves from Greenberg-Castagna and a Basalt regression to these data are shown for comparison.*

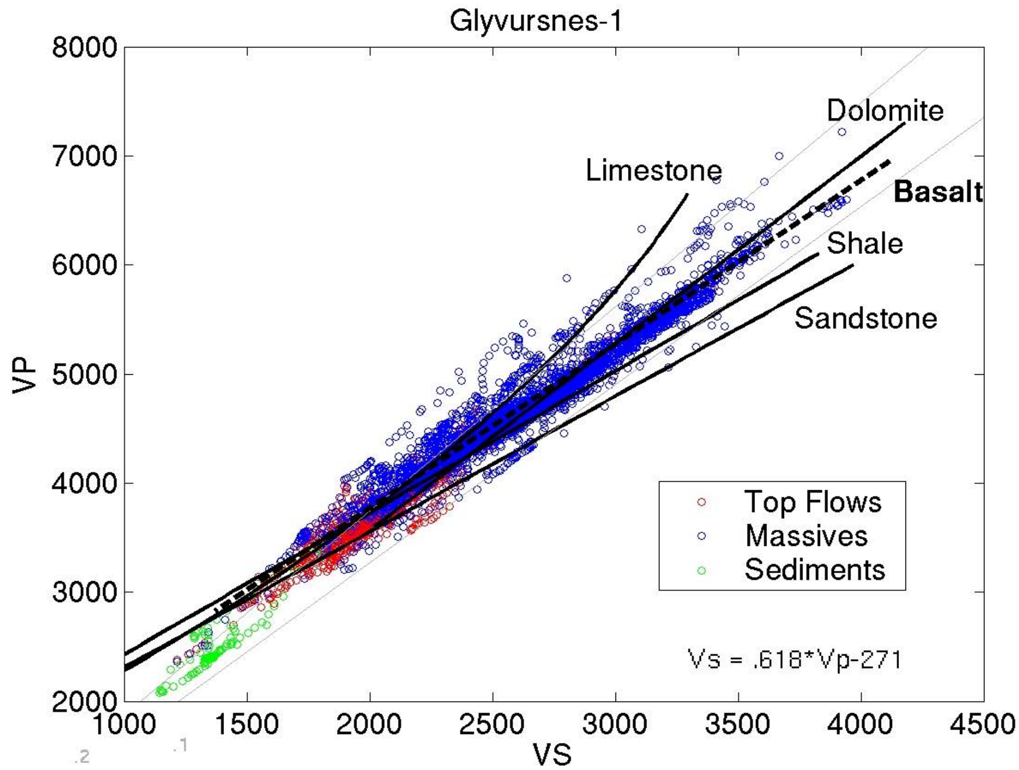

Figure 5. *Sonic Vp vs. Vs for Glyvursnes-1. Empirical curves from Greenberg-Castagna and a Basalt regression to these data are shown for comparison.*

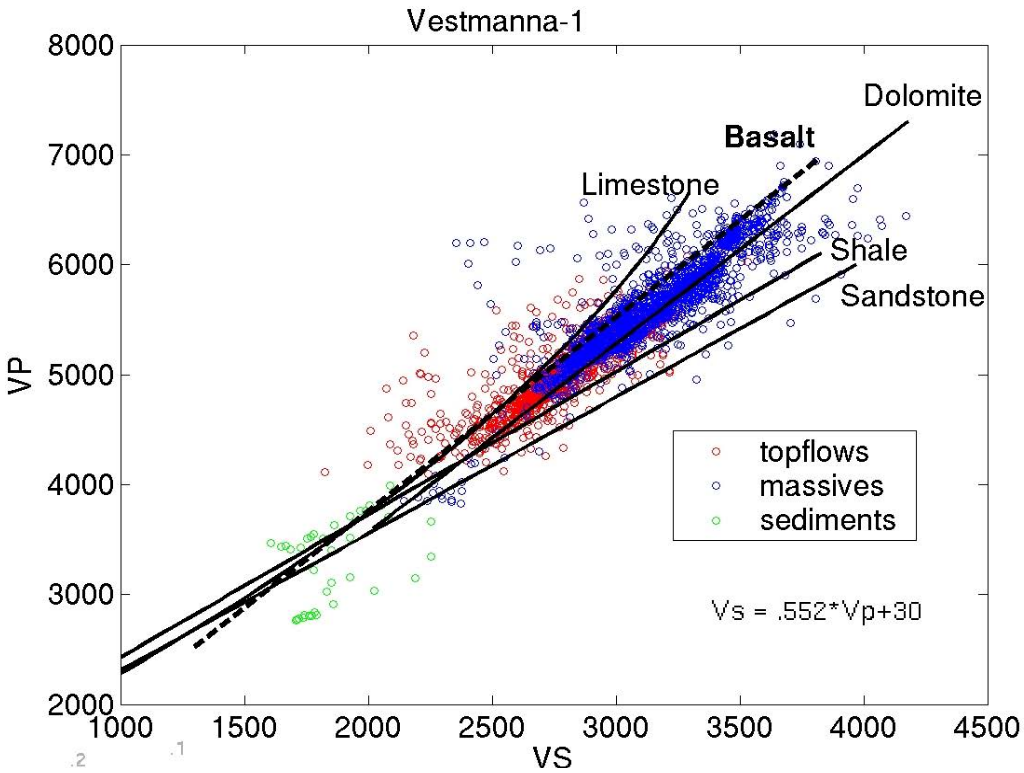

Figure 6. *Sonic Vp vs. Vs for Vestmanna-1. Empirical curves from Greenberg-Castagna and a Basalt regression to these data are shown for comparison.*

Rock physics modelling

In this section, we analyze the observations of Figures 1-5 by comparing them with rock physics models. One set of models represents the pore space as a collection of ellipsoidal inclusions, ranging from flat penny-shaped cracks to spherical pores. The equations that we implement are for the self-consistent formulation of Berryman (1995). The effective rock bulk and shear moduli of an N-phase composite are given by:

$$\sum_{i=1}^{N} x_i(K_i - K^*_{SC})P^{*i} = 0$$

$$\sum_{i=1}^{N} x_i(\mu_i - \mu^*_{SC})Q^{*i} = 0$$

where i refers to the *ith* material, x_i its volume fraction, P and Q are geometric factors given in Table 1, and the superscript ^{*i} on P and Q indicates that the factors are for an inclusion of material i in a background medium with self-consistent effective moduli K^*_{SC} and μ^*_{SC}. These equations are coupled and must be solved by simultaneous iteration.

In the modeling, spherical pores are represented with an aspect ratio of 1; these are the stiffest possible shapes, leading to high velocities for a given porosity. In basalts, these would correspond well to vesicles. Successively smaller aspect ratios represent flattened spherical pores (oblate spheroids), which are successively more compliant. Aspect ratios less than about 0.1 are often referred to as “penny-shaped” cracks. In our application, we assume two phases, mineral and water.

In using these inclusion models, it is important to remember that they are quite idealized, and should not be interpreted too literally. In real rocks there are seldom ellipsoidal pores, though the approximation is probably better in vesicular volcanics than most others. Also, the ellipsoidal models do not explicitly allow for pore connectivity. Nevertheless, these models are useful elastic analogs, and we believe that the trends predicted by them, such as from stiffer pores to more compliant pores, are valid. In our discussion below, the fact that sonic data are consistent with a penny-shaped crack model does not mean that there must be cracks in the rocks. Poorly cemented, compliant grain contacts will yield the same elastic behavior.

Table 1. *Coefficients P and Q for some specific shapes. The subscripts m and i refer to the background and inclusion materials [from Berryman (1995)].*

Inclusion shape	P^{mi}	Q^{mi}
Spheres	$\dfrac{K_m + \frac{4}{3}\mu_m}{K_i + \frac{4}{3}\mu_m}$	$\dfrac{\mu_m + \zeta_m}{\mu_i + \zeta_m}$
Needles	$\dfrac{K_m + \mu_m + \frac{1}{3}\mu_i}{K_i + \mu_m + \frac{1}{3}\mu_i}$	$\dfrac{1}{5}\left(\dfrac{4\mu_m}{\mu_m + \mu_i} + 2\dfrac{\mu_m + \gamma_m}{\mu_i + \gamma_m} + \dfrac{K_i + \frac{4}{3}\mu_m}{K_i + \mu_m + \frac{1}{3}\mu_i}\right)$
Disks	$\dfrac{K_m + \frac{4}{3}\mu_i}{K_i + \frac{4}{3}\mu_i}$	$\dfrac{\mu_m + \zeta_i}{\mu_i + \zeta_i}$
Penny cracks	$\dfrac{K_m + \frac{4}{3}\mu_i}{K_i + \frac{4}{3}\mu_i + \pi\alpha\beta_m}$	$\dfrac{1}{5}\left(1 + \dfrac{8\mu_m}{4\mu_i + \pi\alpha(\mu_m + 2\beta_m)} + 2\dfrac{K_i + \frac{2}{3}(\mu_i + \mu_m)}{K_i + \frac{4}{3}\mu_i + \pi\alpha\beta_m}\right)$

$$\beta = \mu\frac{(3K+\mu)}{(3K+4\mu)} \qquad \gamma = \mu\frac{(3K+\mu)}{(3K+7\mu)} \qquad \zeta = \frac{\mu}{6}\,\frac{(9K+8\mu)}{(K+2\mu)}$$

Effect of mineral properties on inclusion model predictions

When comparing theoretical curves with well log data, we find that the results are very sensitive to the assumed mineral properties. Note, however, that the porosity is the neutron porosity that depends on both the free water in the pore space and the water bound in clay minerals. Consequently, the neutron porosity overestimates the true porosity for basalts where clay minerals occur frequently. This effect is apparent from Figure 7 that shows a minimum porosity for the Lopra-1 well at almost 10% whereas the real minimum porosity for the massive lavas must be close to 0%.

Figure 7 shows plots of Vp vs. Vs, Vp vs. Phi, and Vs vs. Phi for Lopra-1. Superimposed are the predictions of the ellipsoidal inclusion model, for average pore aspect ratios of [1, 0.3, 0.1, 0.03, 0.01]. For these curves, we assumed a mineral bulk modulus similar to pyroxene, $K = 110 GPa$, shear modulus, $\mu = 57 GPa$, and density, $\rho = 3.31 g/cm^3$. From the top two plots, it appears that most of the data fall between aspect ratios ~.03 and ~1. Looking closer, we see that the Vp-Phi plot (top) shows data extending from about half way between the curves for aspect ratios 0.03 and 0.1 to past the curve for aspect ratio ~1; in contrast, the Vs-Phi plot (middle) shows data falling both to lower aspect ratios and to higher aspect ratios than the data for Vp. Hence, there is an inconsistency with the model – it does not make physical sense that the P-waves are seeing different pore aspect ratios than the S-waves. The inconsistency is even more obvious in the plot of Vp-Vs (bottom). Note that data extend to very small aspect ratios, < 0.01. Also, the apparent Vp-Vs trend at high velocities deviates from the trend of the model curves. Another puzzling observation is that the lower porosity rocks, presumably deeper in the well, have pore space that seems to become softer and more crack-like, rather than rounder and stiffer. One way to explain these various model discrepancies is that the Poisson's ratio of the elastic mineral used for modeling is not consistent with the observed Poisson's ratio of the porous rocks.

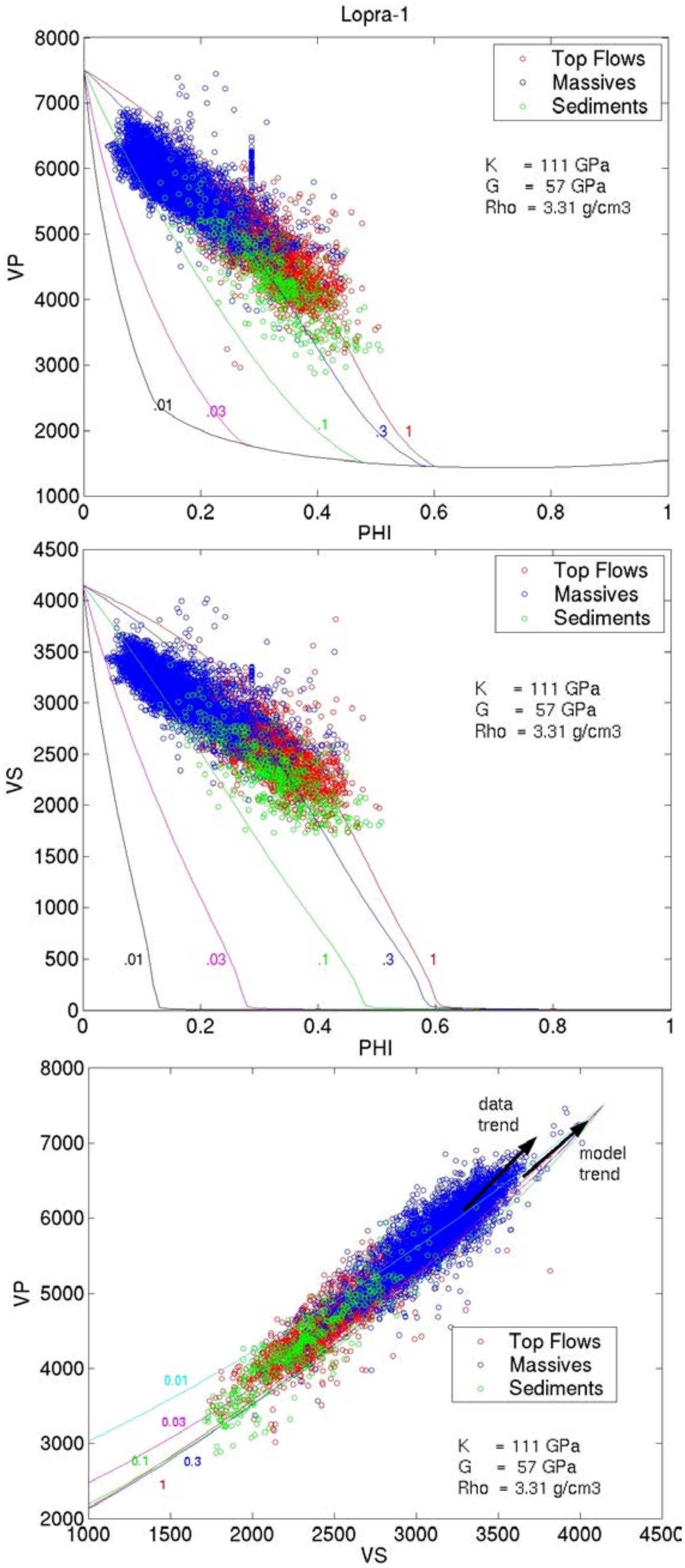

Figure 7. *Comparison of sonic data from Lopra-1 with ellipsoidal inclusion rock model. Inappropriate choice of mineral moduli results in data-model inconsistency.*

Figure 8 shows the same type of plots as in Figure 7, but now with mineral properties adjusted to $K = 120\,GPa$, $\mu = 50\,GPa$, and density, $\rho = 3.31\,g/cm^3$. The moduli were adjusted empirically to find model predictions consistent with both P- and S-wave velocity data. We now observe that the plots of Vp vs. Phi (top) and Vs vs. Phi (middle) show data falling consistently in the aspect ratio range ~.03-1. In the plot of Vp vs. Vs (bottom) it is difficult to conclude much about the range of aspect ratios, because the curves cluster more closely than the scatter in the data. Nevertheless, the model curves capture much better the overall trend of the Vp vs. Vs data.

Figure 9 shows the same type of plots as in Figures 7 and 8, but now for Glyvursnes-1. Here, model consistency with both Vp and Vs requires a different set of mineral properties, $K = 111\,GPa$, $\mu = 57\,GPa$, and density, $\rho = 3.31\,g/cm^3$. In Vestmanna-1 (Figure 10), model consistency requires mineral properties, $K = 120\,GPa$, $\mu = 55\,GPa$, and density, $\rho = 3.31\,g/cm^3$.

In summary, inference of pore shapes corresponding to the log data, based on the ellipsoidal inclusion model is very sensitive to the choice of mineral properties. We observed in Figures 7 and 8 for well Lopra-1 that adjusting the moduli from ($K = 110\,GPa, \mu = 57\,GPa$) to ($K = 120\,GPa, \mu = 50\,GPa$) has a large effect on the consistency of the models with P- and S-wave data. This adjustment caused a change in mineral Vp of less than 1%, but a change in mineral Vs of ~ 6%.

Similarly, model consistency required similar mineral moduli for Lopra-1 and Vestmanna-1, but quite different for Glyvursnes-1. It is difficult to know how much of this discrepancy is a limitation of the idealized ellipsoidal inclusion model. Nevertheless, the Vp/Vs behavior of the data from the three wells shows different trends. Finally, it must be remembered that the modelling so far is limited by the use of the neutron porosity that overestimates porosity. A reduced measure of porosity (e.g. by simply subtracting 10 p.u. from the neutron porosity) would result in smaller estimates of the mineral moduli (see Figs 7 – 10).

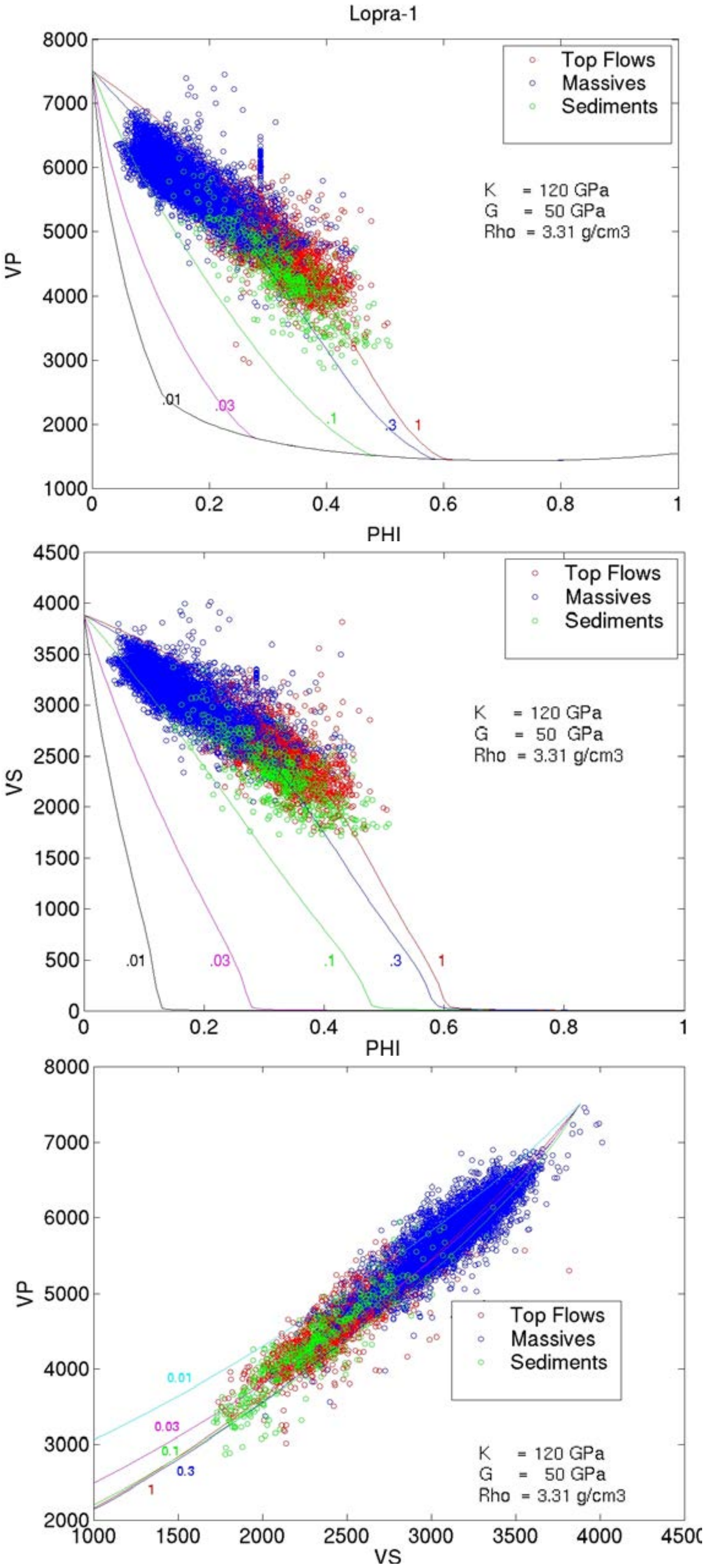

Figure 8. *Comparison of sonic data from Lopra-1 with ellipsoidal inclusion rock model. Adjustment of assume mineral properties gives improved data-model inconsistency.*

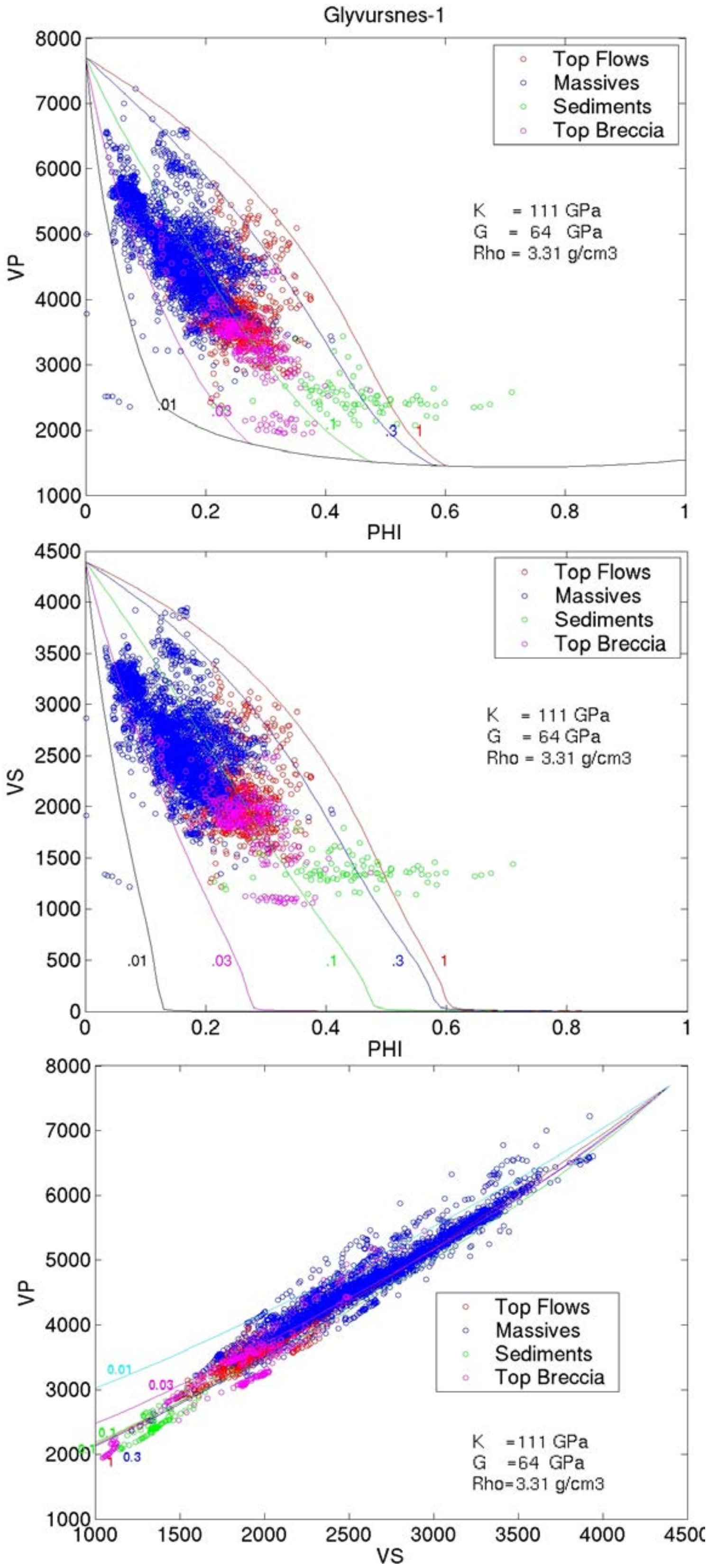

Figure 9. *Comparison of sonic data from Glyvursnes-1 with ellipsoidal inclusion rock model. Adjustment of assume mineral properties gives improved data-model inconsistency.*

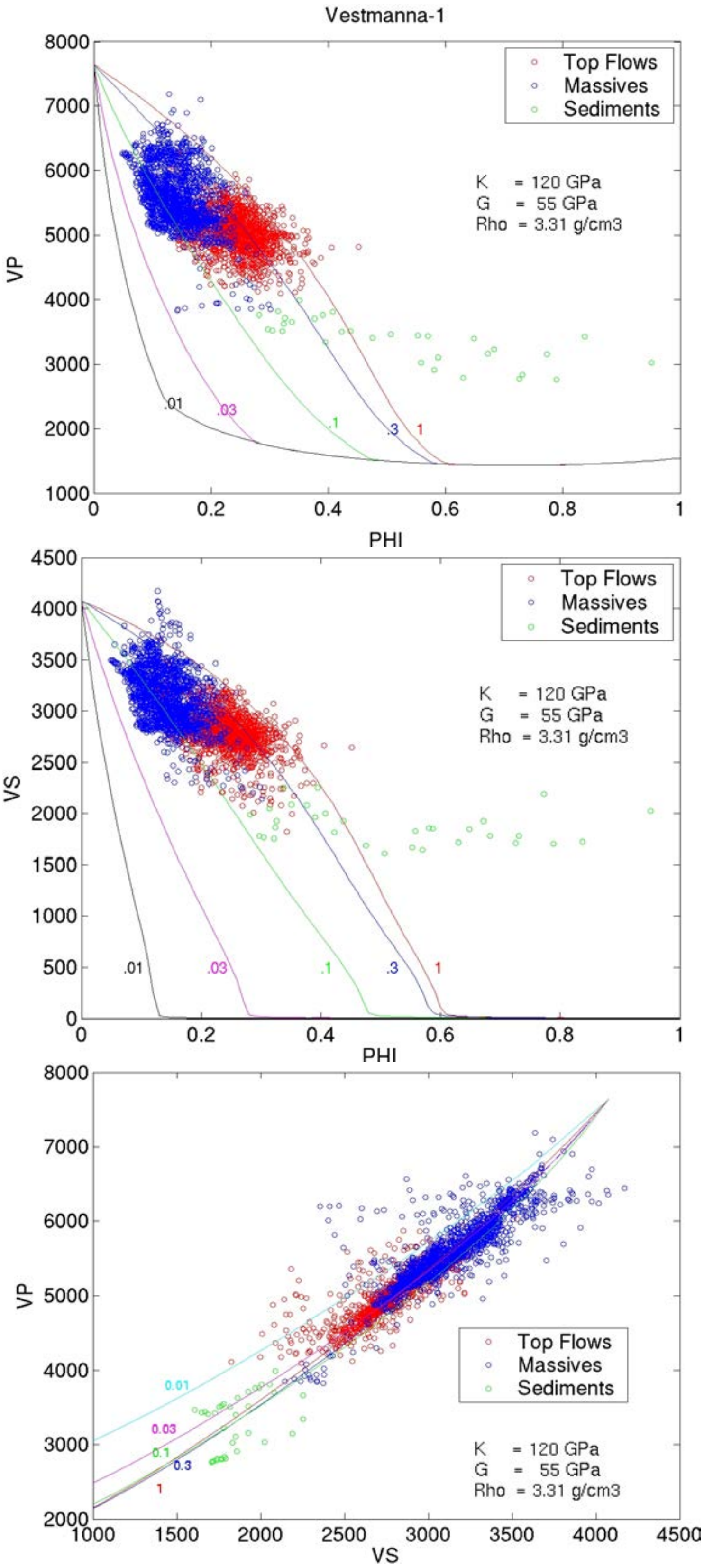

Figure 10. *Comparison of sonic data from Vestmanna-1 with ellipsoidal inclusion rock model. Adjustment of assume mineral properties gives improved data-model inconsistency.*

Comparison among wells in the velocity-porosity planes

Figures 11 and 12 compare plots of sonic Vp vs. Phi and Vs vs. Phi for wells Lopra-1, Glyvursnes-1, and Vestmanna-1. Predictions of the ellipsoidal inclusion model are superimposed, for average pore aspect ratios of [1, 0.3, 0.1, 0.03, 0.01]. As discussed above, slightly different mineral moduli were used for each well, though the mineral Vp is virtually the same. The comparison suggests that the rocks from Lopra-1 span a much larger range of porosities than the other wells; Vestmanna-1 spans the smallest range. Overall, rocks in Lopra-1 appear to have the stiffest pore shapes, while Glyvursnes-1 has the softest pore shapes. Glyvursnes-1 also appears to have the largest range of pore shapes.

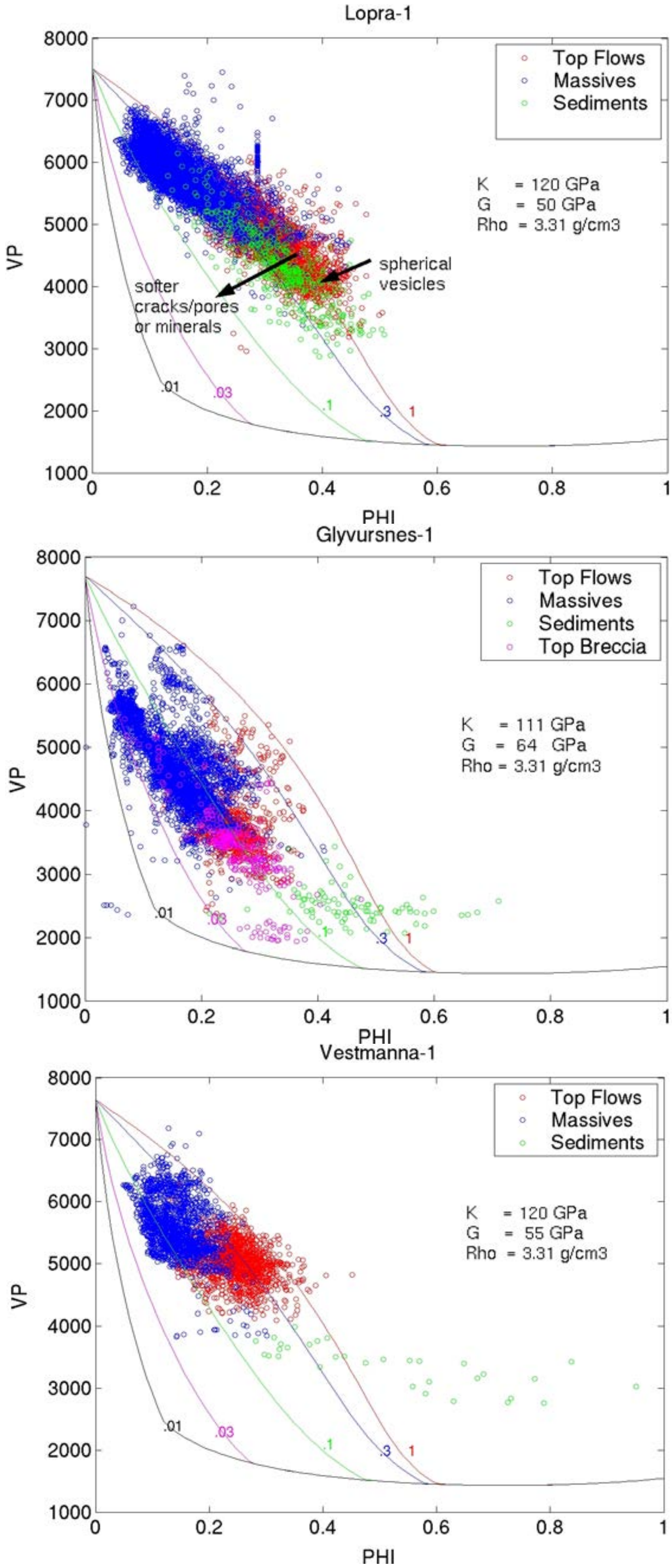

Figure 11. *Comparison of Vp vs. Phi for the three wells.*

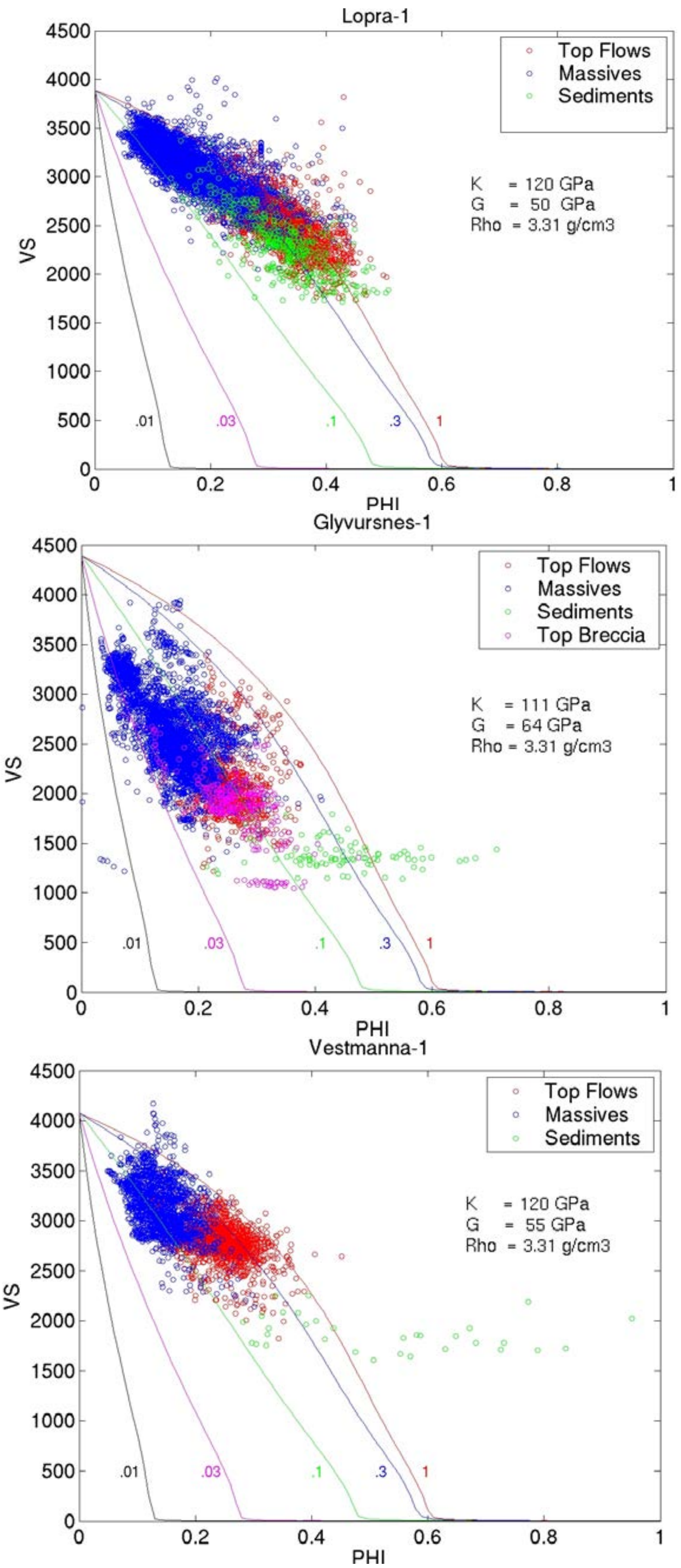

Figure 12. *Comparison of Vs vs. Phi in all three wells.*

Comparison of data with the Hashin-Shtrikman bounds

In Figure 13 we compare sonic Vp vs. Phi data with the Hashin-Shtrikman bounds. The bounds give the maximum and minimum possible effective moduli that can exist for a rock consisting, in this case, of mineral and water. The bounds are given by

$$K^{HS\pm} = K_1 + \frac{f_2}{(K_2 - K_1)^{-1} + f_1\left(K_1 + \frac{4}{3}\mu_1\right)^{-1}}$$

$$\mu^{HS\pm} = \mu_1 + \frac{f_2}{(\mu_2 - \mu_1)^{-1} + \frac{2f_1}{5\mu_1}\frac{(K_1 + 2\mu_1)}{\left(K_1 + \frac{4}{3}\mu_1\right)}}$$

These equations give the *upper* bounds (K^{HS+}, μ^{HS+}) when (K_1, μ_1, f_1) are the bulk modulus, shear modulus and volume fraction of the mineral, and (K_2, μ_2, f_2) are the bulk modulus, shear modulus and volume fraction of the pore fluid. The upper bounds describe the stiffest possible rock. We can visualize a rock falling on or near the upper bounds as being extremely strong and rigid, with extremely stiff pores that are nearly all spherical in shape. Reversing the roles in the equations, we get the *lower* bounds (K^{HS-}, μ^{HS-}) when (K_1, μ_1, f_1) are the bulk modulus, shear modulus and volume fraction of the pore fluid, and (K_2, μ_2, f_2) are the bulk modulus, shear modulus and volume fraction of the mineral. The lower bounds describe the softest possible rock. In the case of basalts, we can think of a rock near the lower bound as full of cracks and fractures to the extend that the rock is essentially falling apart.

The Hashin-Shtrikman bounds are extremely rigorous and reliable, so that when data fall outside the bounds, as we see for a few points in Figure 13, we know that these are either measurement errors, or that the composition is not what we thought.
In Figure 13, we also plot the "modified" upper Hashin-Shtrikman bound (MUHS). For this, we use the same equations shown above, but in this case, (K_1, μ_1, f_1) are the bulk modulus, shear modulus and volume fraction of the mineral, and (K_2, μ_2, f_2) are the bulk modulus, shear modulus and volume fraction of the water-saturated, brecciated rock at the *critical porosity*. The critical porosity for basalts refers to the total porosity at the point when the rock would intercept the lower bound, and therefore fall apart. It has been shown that the MUHS provides an excellent description of the trend extending from the mineral to the critical porosity. While it is not rigorously a bound, it tends to describe the stiffest rocks in the dataset.

The critical porosity value is often determined empirically. For example, sandstones typically have critical porosities at 0.40 and smaller; carbonates have critical porosities above 0.60. In general, a smaller critical porosity implies that the dominant pores leading to rock failure are soft and compliant; a higher critical porosity implies that the dominant pores leading to rock failure are round and stiff. In Figure 13, we observe that the critical porosity for Lopra-1 is about 0.70; for Glyvursnes-1, 0.40; and for Vestmanna-1, 0.60. This is yet another indication that the pore space stiffness is largest in Lopra-1, and smallest in Glyvursnes-1, similar to our conclusions based on the ellipsoidal inclusion models. Note that this analysis is based on the neutron porosity and not true porosity.

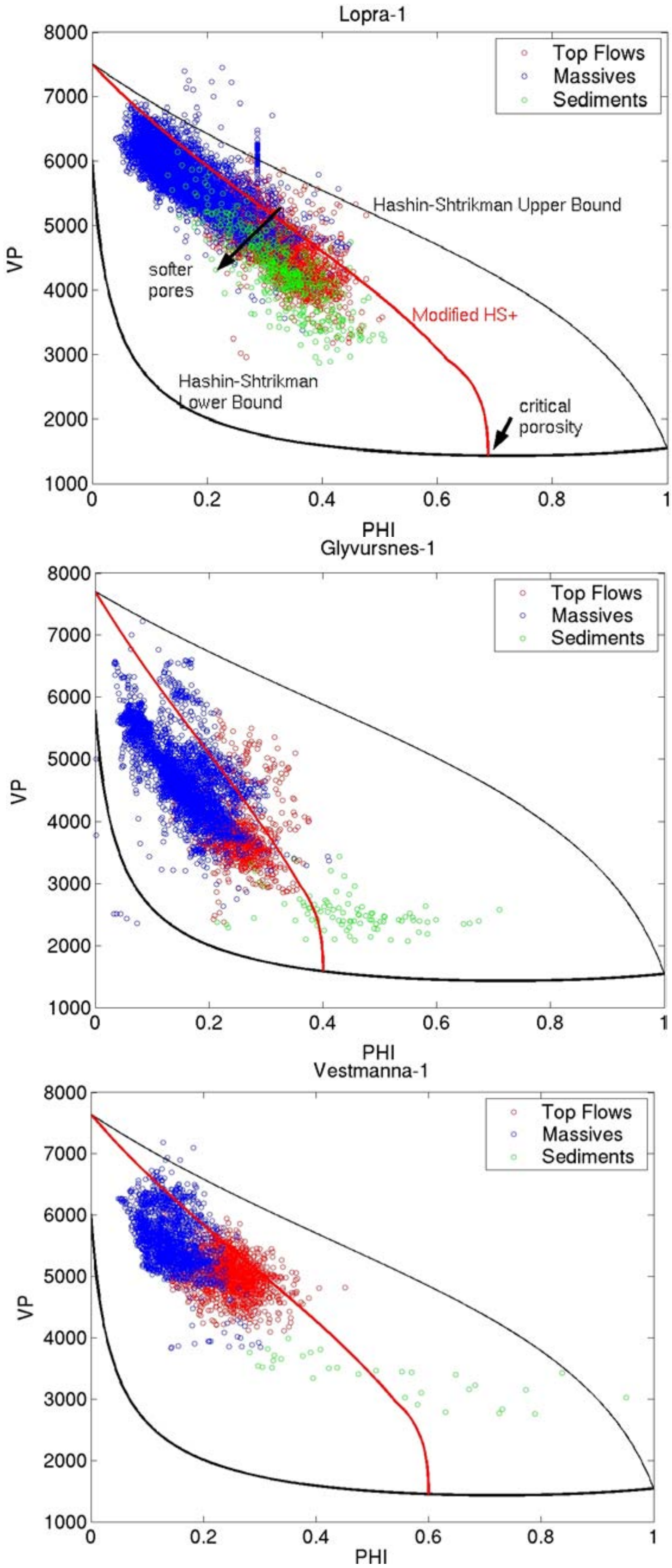

Figure 13. *Comparison of the Hashin-Shtrikman bounds with sonic Vp vs. Phi in all three wells.*

Search for depth trends

Figures 14-16 show plots of Vp vs. Phi, color-coded by depth, for each of the three wells. The top plot in each figure is for the topflow basalts, and the bottom plot is for the massive basalt. Model curves from the ellipsoidal inclusion model are superimposed.
The data from Lopra-1 (Figure 14) show very little evidence of variation of velocity or pore shape with depth. The shallowest data (dark blue) seem to be scattered throughout the data clouds. The very deepest data in both plots do tend to be among the highest velocities.

The data from Glyvursnes-1 (Figure 15) show a pronounced variation of pore aspect ratio with depth. In both the topflows and massives, the shallowest data (dark blue) fall along the lowest aspect ratios, indicating crack-like pore space. The pore space stiffness systematically increases with depth, which could occur from the closing of cracks with increasing overburden stress, or the mineralization of cracks and compliant grain boundaries.
Data from Vestmanna-1 also show a variation of pore space stiffness with depth, but not as simple as in Glyvursnes-1. In both the topflows and the massives, we observe the very shallowest data at low aspect ratios, again indicating crack-like behavior. The aspect ratios increase with the first 400 m of depth, and then decrease abruptly in the last 100 m.

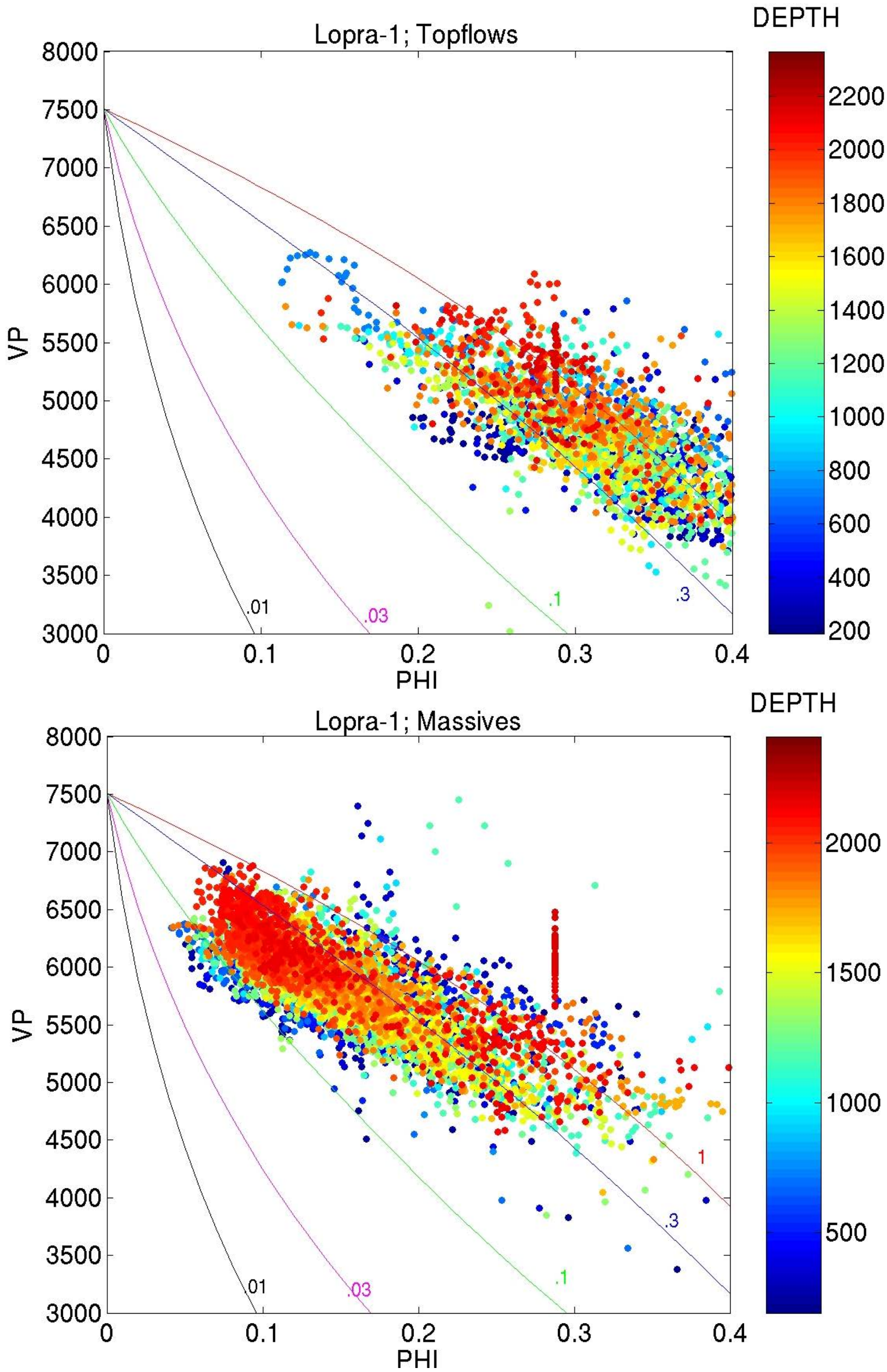

Figure 14. *Sonic Vp vs. Phi, color-coded by depth, in Lopra-1.*

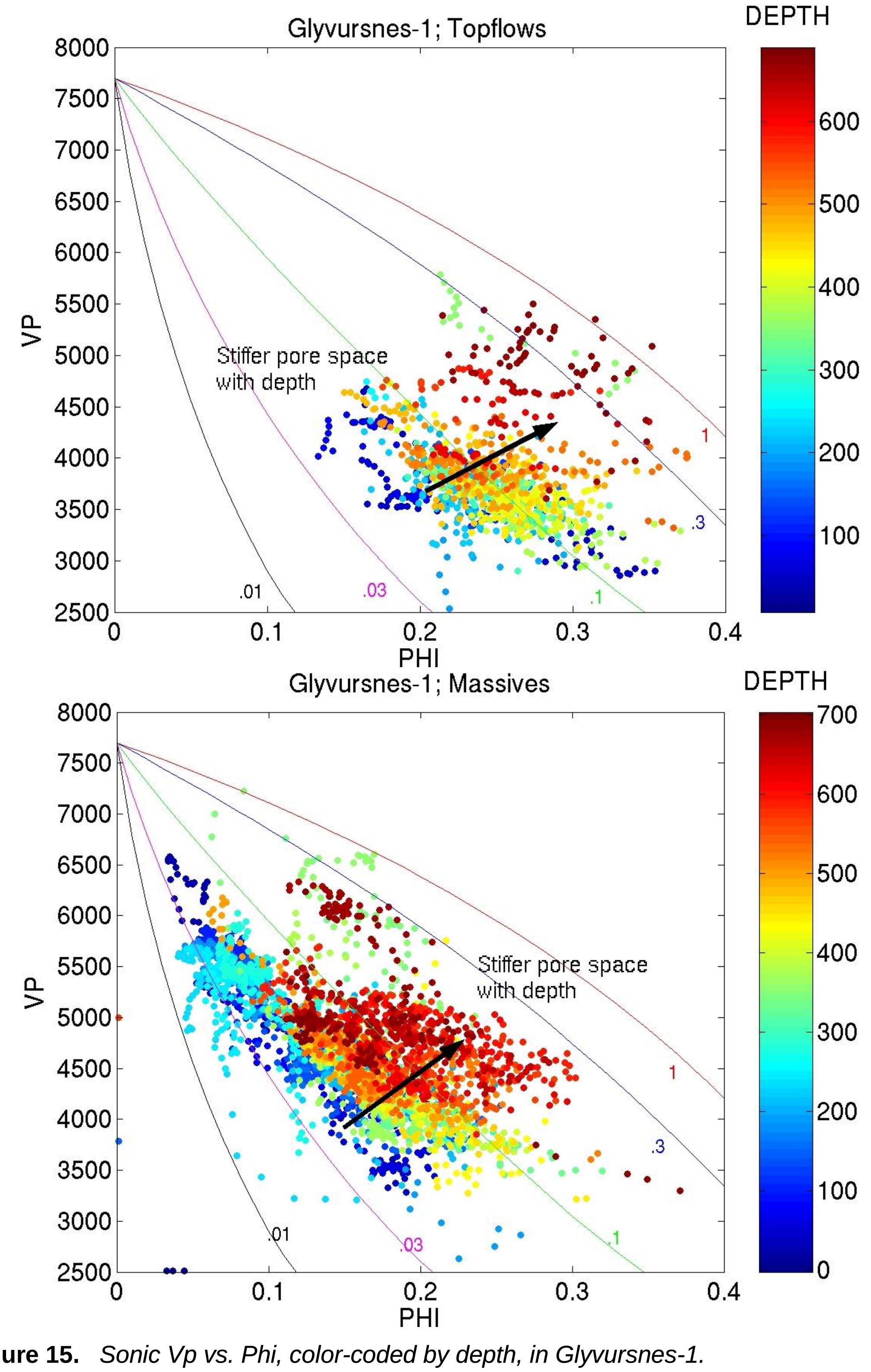

Figure 15. *Sonic Vp vs. Phi, color-coded by depth, in Glyvursnes-1.*

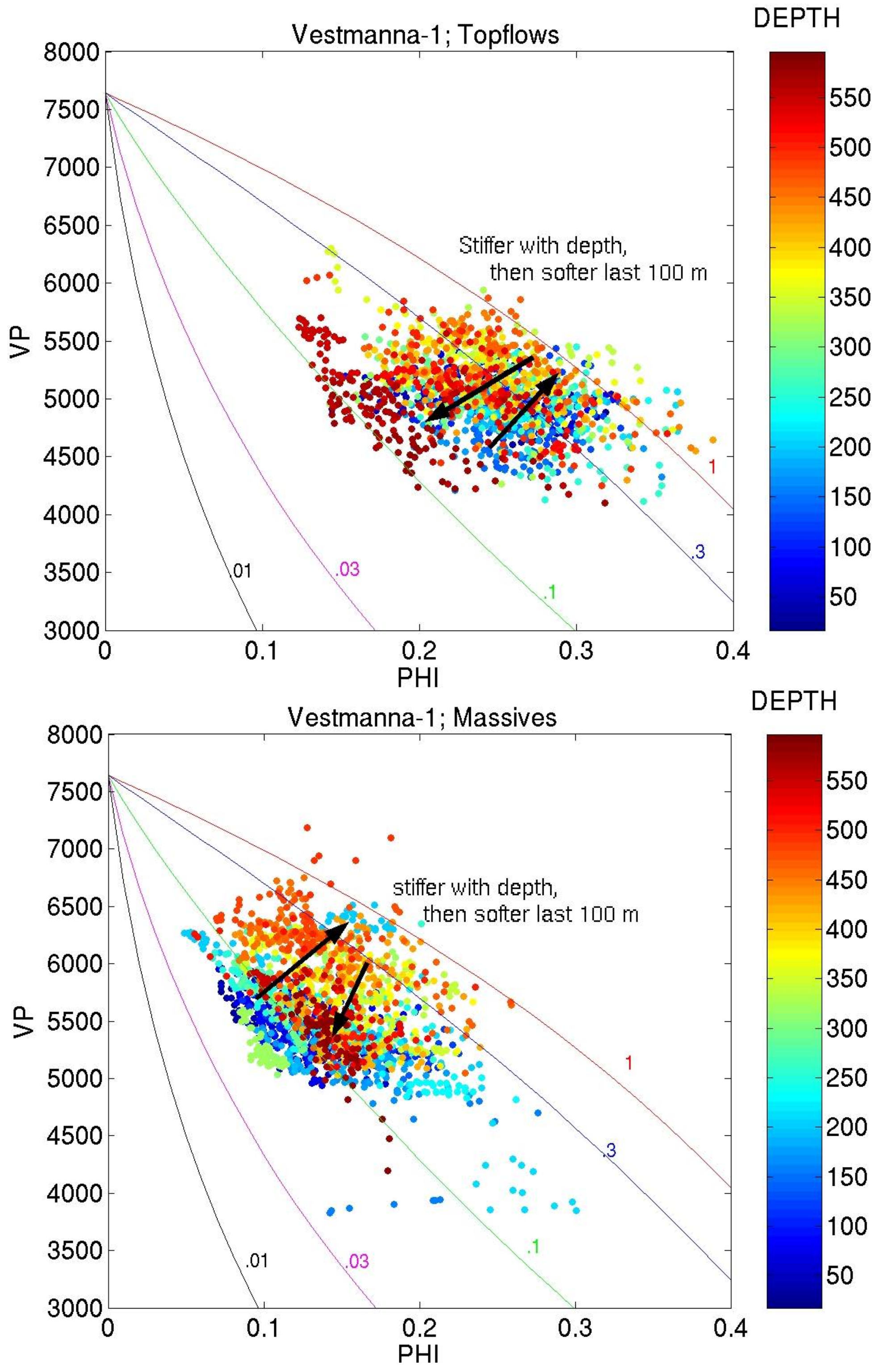

Figure 16. *Sonic Vp vs. Phi, color-coded by depth, in Vestmanna-1.*

Summary

We have examined the sonic behavior from wells Lopra-1, Glyvursnes-1, and Vestmanna-1. In general we observe that the sediment facies have the highest gamma ray and the lowest velocities, while the basalt facies have the highest velocities. Data from Lopra-1 and Vestmanna-1 have similar velocities and Vp/Vs ratios, while Glyvursnes-1 indicates smaller Vp/Vs ratios. Comparison of the sonic data with rock physics ellipsoidal inclusion models suggests that there are slight mineralogical difference among the three wells, indicated by different mineral elastic moduli required for model consistency. It is not obvious how the introduction of quartz, calcite, clay, or zeolites can account for these differences in average mineral moduli. In the future analysis of the data, a correction of the neutron porosity values should be attempted to give a better estimate of the true porosity. Well Lopra-1 showed little correlation of velocity or pore stiffness with depth, though wells Glyvursnes-1 and Vestmanna-1 show a fairly systematic stiffening of the pore space with depth although Vestmanna-1 shows an abrupt change in the lower 100 m of the well.

References

Berryman, J.G., 1995, Mixture theories for rock properties, *in: A Handbook of Physical Constants,* Ahrens, T.J., ed., American Geophysical Union, Washington, 236 pp.

Boldreel,L.O. 2003. Identification and characterization of basalt and sediment units based on wireline logs from the Lopra deep well, Faroe Islands, NE Atlantic Ocean. *EGS General Assembly XXVII.* Nice, France. Abstract EGS02-A-05330,

Greenberg, M.L. and Castagna, J.P., 1992, Shear-wave velocity estimation in porous rocks: theoretical formulation, preliminary verification and applications, *Geophysical Prospecting*, 40, 195-209.

Hald, N. & Waagstein, R. 1984. Lithology and chemistry of a 2-km sequence of Lower Tertiary tholeiitic lavas drilled on Suduroy, Faroe Islands (Lopra-1). *In*: Berthelsen, O. Noe-Nygaard, A. & Rasmussen, J. (eds) *The deep drilling project 1980–1981 in the Faeroe Islands*. Føroya Frodskaparfelag, Torshavn, 15–38.

Japsen, P., Andersen, C., Andersen, H.L., Boldreel, L.O., Mavko, G., Mohammed, N.G., Pedersen, J.M., Petersen, U.K., Rasmussen, R., Shaw, F., Springer, N., Waagstein, R., White, R.S. & Worthington ,M. in press.. Preliminary results of petrophysical and seismic properties of Faroes basalts (SeiFaBa project). In: Doré, A.G.&Vining, B. (eds) *Petroleum Geology: NW Europe and Global Perspectives: Proceedings of the 6th Conference.* Geological Society, London.

Mavko, G., Japsen, P. & Boldreel, L.O. 2004. Preliminary rock physics analysis of basalts in the Lopra-1 well. *GEUS rapport* 2004/96, 11 pp.

Nielsen, P. H., Stefánsson, V. & Tulinius, H. 1984. Geophysical logs from Lopra-1 and Vestmanna-1. *In*: Berthelsen, O., Noe-Nygaard, A. & Rasmussen, J. (eds) *The deep drilling project 1980–1981 in the Faeroe Islands*. Føroya Frodskaparfelag, Torshavn.

Waagstein R. 1983. *Vestmanna well No. 1, Streymoy, Faroe Islands*. Danmarks Geologiske Undersøgelse, intern rapport, København, 40 pp.

Waagstein, R. & Andersen, C. 2004. Well completion report: Glyvursnes-1 and Vestmanna-1, Faroe Islands. Contribution to the SeiFaBa project funded by the Sindri Group. *GEUS rapport* 2003/99, 67 pp.